doi:10.1093/brain/awv328 BRAIN 2016: 139; 242–258 | 242

BRAIN
A JOURNAL OF NEUROLOGY

Frontal white matter hyperintensities, clasmatodendrosis and gliovascular abnormalities in ageing and post-stroke dementia

Aiqing Chen,[1] Rufus O. Akinyemi,[1]* Yoshiki Hase,[1]* Michael J. Firbank,[1] Michael N. Ndung'u,[2] Vincent Foster,[1] Lucy J. L. Craggs,[1] Kazuo Washida,[1] Yoko Okamoto,[1,†] Alan J. Thomas,[1] Tuomo M. Polvikoski,[1] Louise M. Allan,[1] Arthur E. Oakley,[1] John T. O'Brien,[1] Karen Horsburgh,[3] Masafumi Ihara[4] and Raj N. Kalaria[1]

*These authors contributed equally to this work.

†Deceased.

White matter hyperintensities as seen on brain T_2-weighted magnetic resonance imaging are associated with varying degrees of cognitive dysfunction in stroke, cerebral small vessel disease and dementia. The pathophysiological mechanisms within the white matter accounting for cognitive dysfunction remain unclear. With the hypothesis that gliovascular interactions are impaired in subjects with high burdens of white matter hyperintensities, we performed clinicopathological studies in post-stroke survivors, who had exhibited greater frontal white matter hyperintensities volumes that predicted shorter time to dementia onset. Histopathological methods were used to identify substrates in the white matter that would distinguish post-stroke demented from post-stroke non-demented subjects. We focused on the reactive cell marker glial fibrillary acidic protein (GFAP) to study the incidence and location of clasmatodendrosis, a morphological attribute of irreversibly injured astrocytes. In contrast to normal appearing GFAP+ astrocytes, clasmatodendrocytes were swollen and had vacuolated cell bodies. Other markers such as aldehyde dehydrogenase 1 family, member L1 (ALDH1L1) showed cytoplasmic disintegration of the astrocytes. Total GFAP+ cells in both the frontal and temporal white matter were not greater in post-stroke demented versus post-stroke non-demented subjects. However, the percentage of clasmatodendrocytes was increased by >2-fold in subjects with post-stroke demented compared to post-stroke non-demented subjects ($P = 0.026$) and by 11-fold in older controls versus young controls ($P < 0.023$) in the frontal white matter. High ratios of clasmotodendrocytes to total astrocytes in the frontal white matter were consistent with lower Mini-Mental State Examination and the revised Cambridge Cognition Examination scores in post-stroke demented subjects. Double immunofluorescent staining showed aberrant co-localization of aquaporin 4 (AQP4) in retracted GFAP+ astrocytes with disrupted end-feet juxtaposed to microvessels. To explore whether this was associated with the disrupted gliovascular interactions or blood–brain barrier damage, we assessed the co-localization of GFAP and AQP4 immunoreactivities in post-mortem brains from adult baboons with cerebral hypoperfusive injury, induced by occlusion of three major vessels supplying blood to the brain. Analysis of the frontal white matter in perfused brains from the animals surviving 1–28 days after occlusion revealed that the highest intensity of fibrinogen immunoreactivity was at 14 days. At this survival time point, we also noted strikingly similar redistribution of AQP4 and GFAP+ astrocytes transformed into clasmatodendrocytes. Our findings suggest novel associations between irreversible astrocyte injury and disruption of gliovascular interactions at the blood–brain barrier in the frontal white matter and cognitive impairment in elderly post-stroke survivors. We propose that clasmatodendrosis is another pathological substrate, linked to white matter hyperintensities and frontal white matter changes, which may contribute to post-stroke or small vessel disease dementia.

Received April 7, 2015. Revised September 28, 2015. Accepted September 29, 2015. Advance Access publication December 14, 2015

1 Neurovascular Research Group, Institute of Neuroscience, Newcastle University, Campus for Ageing and Vitality, Newcastle Upon Tyne, UK
2 Institute of Primate Research, National Museums of Kenya, Kenya
3 Centre for Neuroregeneration, University of Edinburgh, Chancellor's Building, 49 Little France Crescent, Edinburgh, EH16 4SB, UK
4 Department of Stroke and Cerebrovascular Diseases, National Cerebral and Cardiovascular Center, 5-7-1 Fujishiro-dai, Suita, Osaka 565-8565, Japan

Correspondence to: Professor R. N. Kalaria
Institute of Neuroscience
Newcastle University
Campus for Ageing and Vitality
Newcastle upon Tyne, NE4 5PL, UK
E-mail: raj.kalaria@ncl.ac.uk

Keywords: ageing; clasmatodendrocyte; blood–brain barrier; post-stroke dementia; white matter

Abbreviations: PSD = post-stroke dementia; PSND = post-stroke non-demented

Introduction

Dementia develops in 25–30% of elderly people who survive after stroke (Savva and Stephan, 2010; Allan *et al.*, 2011). Various brain structure changes associated with neurodegenerative dementias such as total cerebral volume, medial temporal lobe atrophy and cortical thinning, also relate to cognitive dysfunction in cerebrovascular disease. However, the pathological substrates associated with cognitive impairment or dementia in cerebrovascular disease remain poorly defined. White matter hyperintensities as seen on brain T_2-weighted MRI have been linked to varying degrees of cognitive impairment (Debette and Markus, 2010). The prevalence and the volume of white matter hyperintensities increase exponentially with age (de Leeuw *et al.*, 2001), and are associated with variable severity of executive dysfunction (DeCarli *et al.*, 1995; Vataja *et al.*, 2003; Bolandzadeh *et al.*, 2012). We previously reported that in older stroke patients, cognitive processing speed and performance as measures of attention are significantly associated with white matter hyperintensity volume, particularly in the frontal lobe regions, whereas memory impairment was associated with the volume of temporal lobe white matter hyperintensities (Burton *et al.*, 2004). It has been widely proposed that many of the cognitive deficits in cerebrovascular dementia are attributed to disruption of the frontal-subcortical circuits (Kalaria and Ihara, 2013).

We have previously shown that myelin density in the white matter was most reduced in vascular dementia compared to Alzheimer's disease and other less prevalent dementias (Ihara *et al.*, 2010). These observations are consistent with the severity of white matter disease and decreased ratios of myelin basic protein and proteolipid protein in subjects with small vessel disease and vascular dementia compared with Alzheimer's disease and ageing controls (Barker *et al.*, 2013). In vascular dementia, the vasoconstrictor endothelin 1 tended to be elevated, possibly reflecting abnormal regulation of white matter perfusion (Barker *et al.*, 2014). However, the precise pathophysiological relationships between white matter changes and cognitive dysfunction are not well understood.

In addition to myelin, axonal and microvascular integrity as well as glial cell reactivity have been of interest as possible substrates of the white matter that correlate with the severity of white matter hyperintensities and cognitive impairment. Astrocytes, as one of the fundamental glial cells in brain tissue (Abbott *et al.*, 2006), are important for creating a homeostatic environment and providing energy for oligodendrocytes and axons (Funfschilling *et al.*, 2012). During ischaemia, when acidosis and energy failure occurs, astrocytes can undergo clasmatodendrosis, and cells become amoeboid in shape (Penfield, 1928; Friede and van Houten, 1961). Clasmatodendrosis is further characterized by cytoplasmic swelling and vacuolation of the astrocyte soma, with beading and fragmentation of their dendritic processes, leading to irreversible injury via an autophagic process (Qin *et al.*, 2010). The alterations in cell morphology are directly related to changes in cell function (Hulse *et al.*, 2001; Hinson *et al.*, 2007). Clasmatodendrosis was previously described in various conditions including acute hypoxic-ischaemic injury (Gelot *et al.*, 2009), epilepsy (Kim *et al.*, 2011), and neuromyelitis optica (Tradtrantip *et al.*, 2012; Misu *et al.*, 2013). It was also demonstrated in the white matter of patients with Binswanger's leukoencephalopathy and mixed dementia (Alzheimer's disease combined with cerebrovascular disease) (Tomimoto *et al.*, 1996, 1997) and described in a patient exhibiting severe white matter hyperintensities with autopsy-confirmed mixed dementia (Sahlas *et al.*, 2002) but not necessarily associated with demyelination or neurodegeneration (Popescu *et al.*, 2010). However, clasmatodendrosis has not been evaluated in the development of dementia in cerebrovascular disease.

With the hypothesis that gliovascular interactions are disrupted in individuals who exhibit a high burden of white

matter hyperintensity volume, we explored the incidence of clasmatodendrosis in relation to the cerebral microvasculature in the white matter of elderly stroke survivors, who had developed dementia compared to those who remained cognitively stable and older controls. To further test the hypothesis and verify if the phenomenon was associated with disruption of gliovascular interactions or breach of the blood–brain barrier in the white matter (Wardlaw *et al.*, 2009), we evaluated perfused post-mortem brain tissue from non-human primates subjected to cerebral hypoperfusion.

Materials and methods

Subjects and dementia diagnoses

Stroke patients taking part in the white matter hyperintensities imaging investigation were from a previously described cohort, which was followed longitudinally (Allan *et al.*, 2011). Patients were comprehensively assessed at 3 months post-stroke using a standardized battery comprising medical history, Mini-Mental State Examination (MMSE) score, assessment of neurological deficits, blood screen and review of CT brain scan undertaken at the time of stroke, and were excluded if they: (i) had significant physical illness and disabilities that precluded neuropsychological evaluation (e.g. visual impairment, aphasia, hemiparesis affecting the hand used for writing); (ii) had a diagnosis of dementia according to DSM-IIIR (Diagnostic and Statistical Manual of Mental Disorders) criteria; or (iii) declined to take part. Subjects underwent an annual clinical and cognitive assessment. DSM-IIIR criteria were used because they include a general definition for dementia, unlike DSM-IV, which presumes aetiology, as we were interested in post-stroke dementia regardless of cause. The total number of MRI scans was limited by cost to ~100, so not all subjects were approached. Eligible subjects were consecutively invited to have an MRI scan until 106 had agreed. The analysis here is a subset looking at frontal white matter hyperintensities as a function of time to dementia or death (Table 1). The analysis was performed in scans from 41 decliners, who developed dementia and 65 stable post-stroke survivors. Following full explanation and discussion of the study, patients gave their consent to the evaluations, with additional assent from the next of kin. Ethical approval and permission to progress this study using donated human brain was granted by the Newcastle and North Tyneside 1 Research Ethics Committee.

MRI acquisition and white matter hyperintensity volumes

One hundred and six subjects were imaged using a 1.5 T GE Signa scanner (General Electric). Volume of white matter hyperintensities was obtained from the baseline MRI images (Fig. 1) using previously validated automated software (Firbank *et al.*, 2012). Briefly, spm99 (http://www.fil.ion.ucl.ac.uk/spm) was used to segment the brain from the FLAIR images. Volumes of white matter hyperintensities were then determined by applying an intensity threshold of 1.45-times the modal intensity for each slice to segment the white matter hyperintensities. The accuracy of this was checked visually for each subject and the total white matter hyperintensities volume in the whole brain was calculated. Values in Table 1 are white matter hyperintensities (in ml) for ease of interpretation; however, for the statistical analysis, we calculated the ratio of white matter hyperintensity volume to total brain volume, and to produce normally distributed data we performed log transformation. Subjects were followed up for a mean of 4.0 (SD 2.5) years to last dementia assessment, and 5.9 (SD 2.3) years for deaths. All subjects (apart from two) were followed-up until either death or 9 years after initiation of the study. Of those whose final status was 'without dementia', 32 (74%) out of the 43 who died and 23 (64%) of the 36 still alive had dementia assessment within 1 year of their last recorded vital status.

Neuropathological examination

Brains were retrieved from a total of 40 post-stroke survivors who came to autopsy. Fourteen subjects, who were scanned in life were included in this cohort (Table 2). In addition, we analysed brains from elderly controls, who were age-matched to subjects with post-stroke dementia (PSD) and post-stroke non-demented subjects (PSND), and also a further group of younger controls to demonstrate the effects of ageing alone. Table 2 also provides the final MMSE and the revised Cambridge Cognition Examination (CAMCOG) battery scores of the relevant subjects. Stroke survivors who did not meet DSM-IIIR or IV criteria for dementia and had MMSE scores >25 and CAMCOG scores >85 were designated as 'post-stroke survivors with no dementia'. In the majority of cases, bronchopneumonia was recorded as the cause of death.

Neuropathological assessment was carried out as described previously using standardized protocols (Kalaria *et al.*, 2004; Ihara *et al.*, 2010; Allan *et al.*, 2011; Gemmell *et al.*, 2012). Macroscopic infarcts, detected by visual inspection while dissecting the brain, were subsequently confirmed by light microscopy. Haematoxylin and eosin staining was used for assessment of structural integrity and infarcts, Nissl and Luxol fast blue staining for cellular patterns and myelin loss, Bielschowsky's silver impregnation and immunohistochemical analysis of amyloid-β deposition using antibodies to amyloid-β (4G8, 1:1000, Signet) for the Consortium to Establish a Registry for Alzheimer's Disease (CERAD) rating of neuritic plaques, Gallays for Braak staging of neurofibrillary tangles. Deposition of hyperphosphorylated tau with the AT8 antibody (1:1000, Monoclonal Innogenetics) was further scored using the semi-quantitative approach as described previously (Lace *et al.*, 2009). Vascular pathology scores were derived from the presence of vascular lesions in brain areas, including the frontal lobe at the level of the olfactory bulbs, temporal lobe at the level of the anterior hippocampus, and basal ganglia at the level of mamillary body. Lesions including arteriolosclerosis, fibrinoid necrosis, perivascular spacing and haemosiderin leakage and tissue changes including lacunes, microinfarcts, microhaemorrhages and myelin loss in the deep and juxtacortical white matter, and cortical micro (<0.5 cm) and large (>0.5 cm) infarcts were recorded with increasing severity resulting in greater scores (Deramecourt *et al.*, 2012).

Tissues from control subjects had occasional ageing-related pathology and were classified having 'no pathological diagnosis' (Table 2). Tissue showing any evidence of infarction was

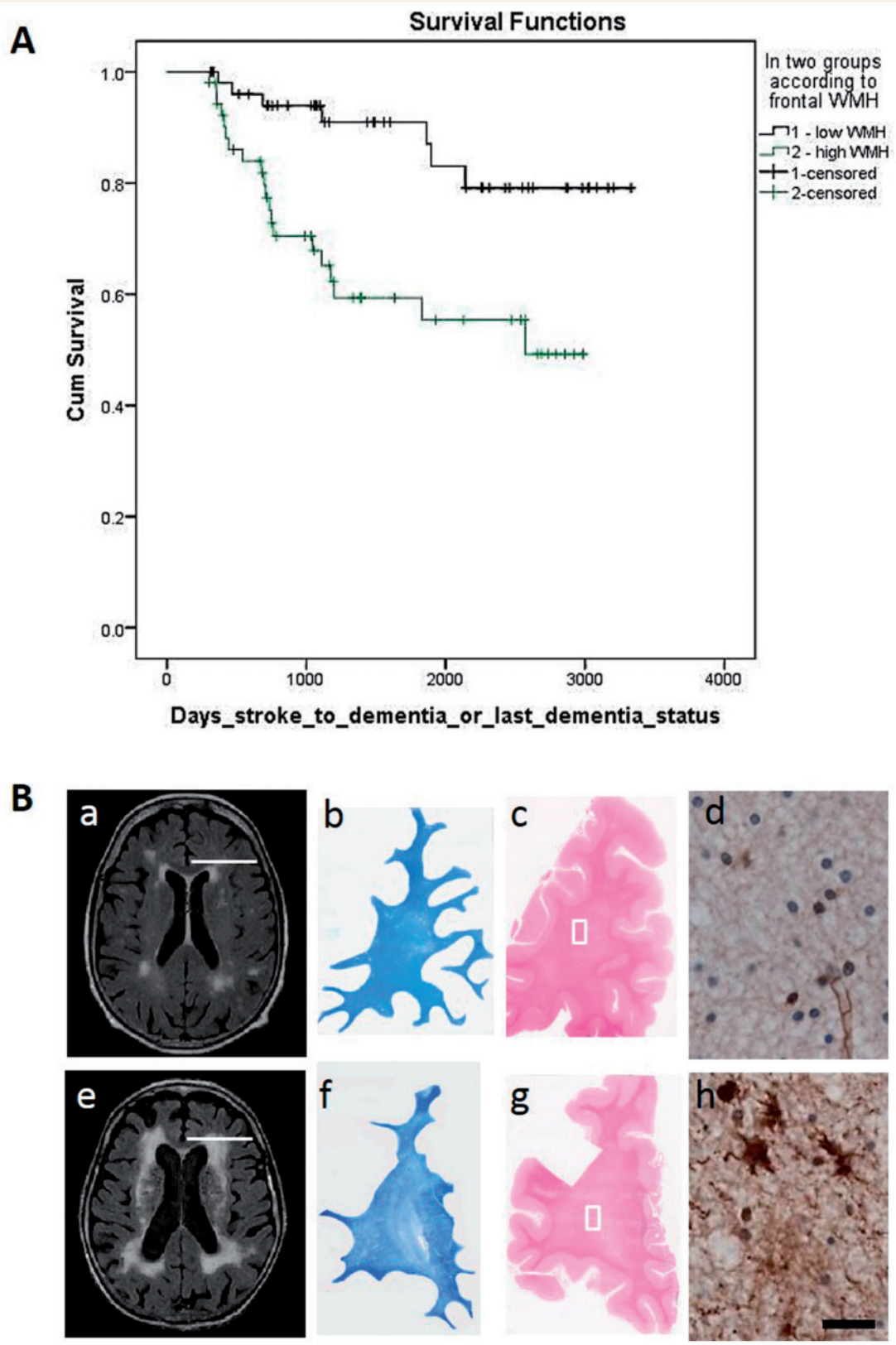

Figure 1 Frontal white matter hyperintensities and associated pathology in stroke survivors. (**A**) Survival curves show progression time to dementia by the presence of frontal white matter hyperintensities volume in non-demented (PSND, *top*) and demented (PSD, *bottom*) subjects. The mean number of days from stroke to dementia in the non-demented and DSM IV demented groups was 1483 ± 922 and 1059 ± 676 ($P = 0.001$). (**B**) MRI (**a** and **e**) in life and coronal sections (**b–d** and **f–h**) demonstrate the extent of differential white matter changes in subjects with PSND (**b–d**) and PSD (**f–h**) from the cohort described in **A**. [**B**(**a** and **e**)] Typical white matter hyperintensity volume differences on MRI with

excluded. Patients with any type of dementing illness were also excluded. In PSD cases, a clinical diagnosis of vascular dementia was made when there were multiple or cystic infarcts, lacunae, microinfarcts and small vessel disease, and Braak stage ⩽IV (Kalaria *et al*., 2004). Mixed dementia was classified when there was significant vascular pathology coupled with appropriate levels of neurofibrillary pathology (Braak staging) and neuritic plaques (CERAD rated) (Kalaria *et al*., 2004).

Three vessel occlusion model and neuropathological analysis in non-human primates

Post-mortem brain tissues were obtained from adult baboons (*Papio anubis*) weighing 16–20 kg (7–12 years old), housed at the Institute of Primate Research, National Museums of Kenya. These non-human primates used widely for stroke research also develop Alzheimer's disease pathology (Ndung'u *et al*., 2012), were part of a study to understand the sequelae of brain changes during cerebral hypoperfusion. This study was performed in collaboration with Kyoto University (Y.H., K.W., Y.O. and M.I.). The animals were subjected to permanent occlusion of both the internal carotid arteries and the left vertebral artery for survival periods of 1, 3, 7, 14, 21 and 28 days (n = 4–7 each group). Following such three-vessel occlusion, temporary mild hemiparesis was evident in all the animals. Animals were euthanized on the designated day and the brains (200–300 g) were retrieved after perfusion fixation. Subsequent to further immersion fixation period of 4–6 weeks, 1-cm thick coronal slices of the brain were processed for extensive histopathological analysis and quantitative evaluation in the same manner as the human post-mortem cases (Ihara *et al*., 2010; Deramecourt *et al*., 2012). We used routine tinctorial stains and immunohistochemistry on 10-μm thick sections of the whole coronal face to assess pathology in the white matter. This included evaluation for changes in myelin (Luxol fast blue), endothelial integrity (haematoxylin and eosin, glucose transporter type 1 (GLUT1, encoded by *SLC2A1*), basement membrane (collagen IV, COL4), the

Table 1 Neuroimaging study subject characteristics and survival to dementia predictors stratified by age in a multivariate cox model

Age at baseline	79.8 (4.1)	n = 106
Gender F:M	57:49	
Deceased during follow-up	60 (57%)	
Developed dementia during follow-up	27 (25%)	
MMSE	26.2 (2.7)	
CAMCOG-R	84.4 (8.5)	
MTA	2.7 (1.8)	
White matter hyperintensity, ml	2.1 (1.8)	
Total brain volume	1009 (82.4)	
Oxford Stroke Classification (LACS/PACS/TACS/POCS/unknown)	35/42/5/17/7	
	HR (95% CI)	***P*-value**
Significant neuroimaging predictor		
MTA	1.40 (1.07 to 1.85)	0.016
Log (frontal white matter hyperintensities / total brain volume)	1.88 (1.05 to 3.36)	0.034
AIREN bilateral thalamic lesions	9.18 (2.36 to 35.63)	0.001
Significant neuroimaging predictor + cognitive score		
MTA	1.32 (1.00 to 1.74)	0.054
Log (frontal white matter hyperintensities / total brain volume)	1.68 (0.92 to 3.05)	0.09
AIREN bilateral thalamic lesions	4.58 (1.19 to 17.70)	0.027
CAMCOG-R	0.93 (0.89 to 0.98)	0.004

Oxford community stroke project (OCSP) classification: there were no significant differences between stroke territory distributions between PSND and PSD cases ($P > 0.05$). CAMCOG = Cambridge Assessment for mental and cognition; LACS = lacunar stroke; na = not available; PACS = partial anterior circulation stroke; POCS = posterior circulation stroke; TACS = total anterior circulation stroke; AIREN = relevant imaging change meets imaging criteria as specified in the National Institute of Neurological Disorders and Stroke Association/Internationale pour la Recherche *et al*' Enseignement en Neurosciences (NINDS/AIREN) criteria; CAMCOG-R = Cambridge Cognitive Assessment-revised; GDS = Geriatric Depression 15 point scale; MTA = medial temporal lobe atrophy rating; MMSE = Mini-Mental State Examination; TIA = transient ischaemic attack.

Figure 1 Continued

FLAIR in PSND (**a**) and PSD (**e**) subjects. Examples are from females aged 86 and 90 years. [**B**(**b**, **c**, **f** and **g**)] Coronal sections from the magnetic resonance scanned cases stained with Luxol fast blue and haematoxylin and eosin. Diffuse myelin changes are more evident in the PSD coronal sections. [**B**(**d** and **h**)] Adjacent sections from the same cases stained for fibrinogen immunoreactivity. [**B**(**h**)] shows diffuse immunoreactivity and also demonstrates in astrocytes blood–brain barrier leakage of proteins. The location of coronal sections in **B**(**b**, **c**, **f** and **g**) are shown by the white line in the axial MR scans in **B**(**a** and **e**). Images in **B**(**d** and **h**) are from the frontal white matter areas represented by boxes in the haematoxylin and eosin-stained sections **B**(**c** and **g**). Scale bar = 10 μm. WMH = white matter hyperintensities.

Table 2 Pathological study subject demographics and clinical features

Group	Young controls	Old controls	PSND	PSD
n	10	15	23	17
Age (years)*	61.1 ± 2.3	84.2 ± 2.6	84.0 ± 0.8	87.6 ± 1.4
Gender (F:M)	5:2	13:2	8:15	10:7
PMD (h)	46 ± 9	39 ± 6	37 ± 4	39 ± 6
Clinical and psychometric features				
MMSE (0–30)*	Na	na	27.3 ± 0.3	16.5 ± 1.2
Total CAMCOG (0–106)*	na	na	88.8 (83–98)	62.5 (24–80)
Time from baseline to death (months)	–	–	63.5 (22)	64.4 (14)
Memory subscore (/27)*	–	–	21.4 (2.8)	15 (4.3)
Executive function subscore (/28)*	–	–	16.6 (1.2)	11.1 (1.9)
Clinical Dementia Rating (CDR)*	–	–	0.1 ± 0.4	1.28 (0.25)
Hemisphere with visible change or not on CT; None, right, left, both	–	–	14, 3, 2, 4	8, 4, 1, 4
OCSP stroke classification LACS, PACS, POCS, TACS	–	–	13, 4, 2, 4	8, 4, 1, 4
Pathological markers				
Braak Staging range[a]	0–I	I–III	I–IV	I–IV
Tau (AT-8) Score 0–6 (range)[b]	–	1.3 (1–3)	1 (1)	1.3 (1–3)
CERAD Score range[c]	–	1–2	1–2	1—3
Vascular pathology score (range)[d]	–	8.1 (8–10)	13.5 (13–14)	13.3 (9–17)
White matter score (SEM)[e]	–	1.5 (0.3)	2.5 (0.4)	2.4 (0.4)
Myelin index (SEM)[e]	–	25 (2)	30 (4)	34 (3)
Sclerotic index (SEM)[e]	–	0.40 (0.03)	0.44 (0.02)	0.40 (0.01)
Perivascular spacing (SEM)[e]	–	83 (8.6)	82 (4.6)	82 (5.2)

Numbers represent mean values (±2 SEM) and where given with the range of values in parentheses. The causes of death included bronchopneumonia, cardiac arrest and carcinoma with no particular distribution in any group. The time period (weeks) of tissue fixation was in range 8–40 weeks for all the cases. There was no pathological diagnosis in young or old controls.

[a]Braak staging in >90% of the cases was below III. None of the cases had neurofibrillary pathology above stage V (Kalaria *et al*., 2004).

[b]Hyperphosphorylated Tau scores were derived by immunostaining sections with AT-8 antibody using a visual rating score from 0 to 6 in order of severity. AT8 immunoreactivity was not significantly different between PSND and PSD.

[c]CERAD scores were determined as 1 = sparse, 2 = moderate and 3 = severe.

[d]Vascular pathology scores were derived as described previously (Deramecourt *et al*., 2012).

[e]Data for the frontal lobe only.

*Significance: $P < 0.05$ between young and older controls and between the PSND and PSD groups.

CERAD = Consortium to Establish a Registry for Alzheimer's disease score; *n* = number; na = not available; OCSP = Oxford Community Stroke Project; PMD = post-mortem delay; LACS = lacunar stroke; PACS = partial anterior circulation stroke; POCS = posterior circulation stroke; TACS = total anterior circulation stroke.

blood–brain barrier (fibrinogen), the key water channel protein (AQP4) and astrocytes (GFAP). The Institute of Primate Research (IPR) internal review board of the National Museums granted ethical approval and permission for this entire study.

Immunohistochemistry and immunofluorescent labelling

Ten- or 6-μm thick paraffin wax embedded coronal sections from PSND, PSD and non-stroke controls were immunostained with various primary monoclonal or polyclonal antibodies: rabbit anti-GFAP antibody (1:1000, Z0334, Dako), mouse anti-GFAP (1:50, clone 6F2, M0761, Dako), aldehyde dehydrogenase 1 family, member L1 (ALDH1L1; 1:100 in 0.1% Trion^{TM} X-100–PBS for immunofluorescence, clone 7G8, mouse antibody, 14-9595, eBioscience), aquaporin 4 (AQP4; 1:50, rabbit antibody, 16473-1-AP, Proteintech), Delta Like-1 (DLL1; 1:1000, goat antibody, Ab# 76655 Abcam), LC3 (autophagic vacuoles; 1:100, rabbit antibody, AP1801a Abgent), Poly (ADP-ribose) polymers (PARP1 of 2nd Zinc finger of DNA binding domain, 1:30, polyclonal rabbit, Prof. Alex Burkle, University of Konstanz, Germany) and fibrinogen (1:2000, rabbit antibody, A0080, Dako). Tissue sections first underwent antigen retrieval by heating in the microwave with citrate buffer for 12 min before being quenched with Tris-buffered saline and 3% hydrogen peroxide. Sections were then blocked with serum derived from the species in which the secondary antibody was generated, before being immunostained with the primary antibody overnight at 4°C.

Standard colour immunohistochemistry was performed using the Vectastain ABC System. Quantification was performed following the general pattern we established previously for either parenchymal or cellular protein immunoreactivity (Ihara *et al*., 2010; Foster *et al*., 2014). Briefly for GFAP+ cells, at least 20 images were acquired randomly from areas of the deep white matter in coronal sections (Fig. 2), using a Leitz DIALUX 20 brightfield microscope coupled to a lumenera infinity digital camera at ×6.3 magnification. Using ImageJ, the total GFAP+ cells and cells showing features of clasmatodendrosis (swollen cell body and beaded processes) were counted from both frontal and temporal deep white matter in each case, with the percentage of clasmatodendrotic astroglia calculated and expressed as a ratio. To verify that only astrocytic cells were targeted, we determined that GFAP cell counts per 0.5 mm^2 correlated positively with GFAP staining per unit area

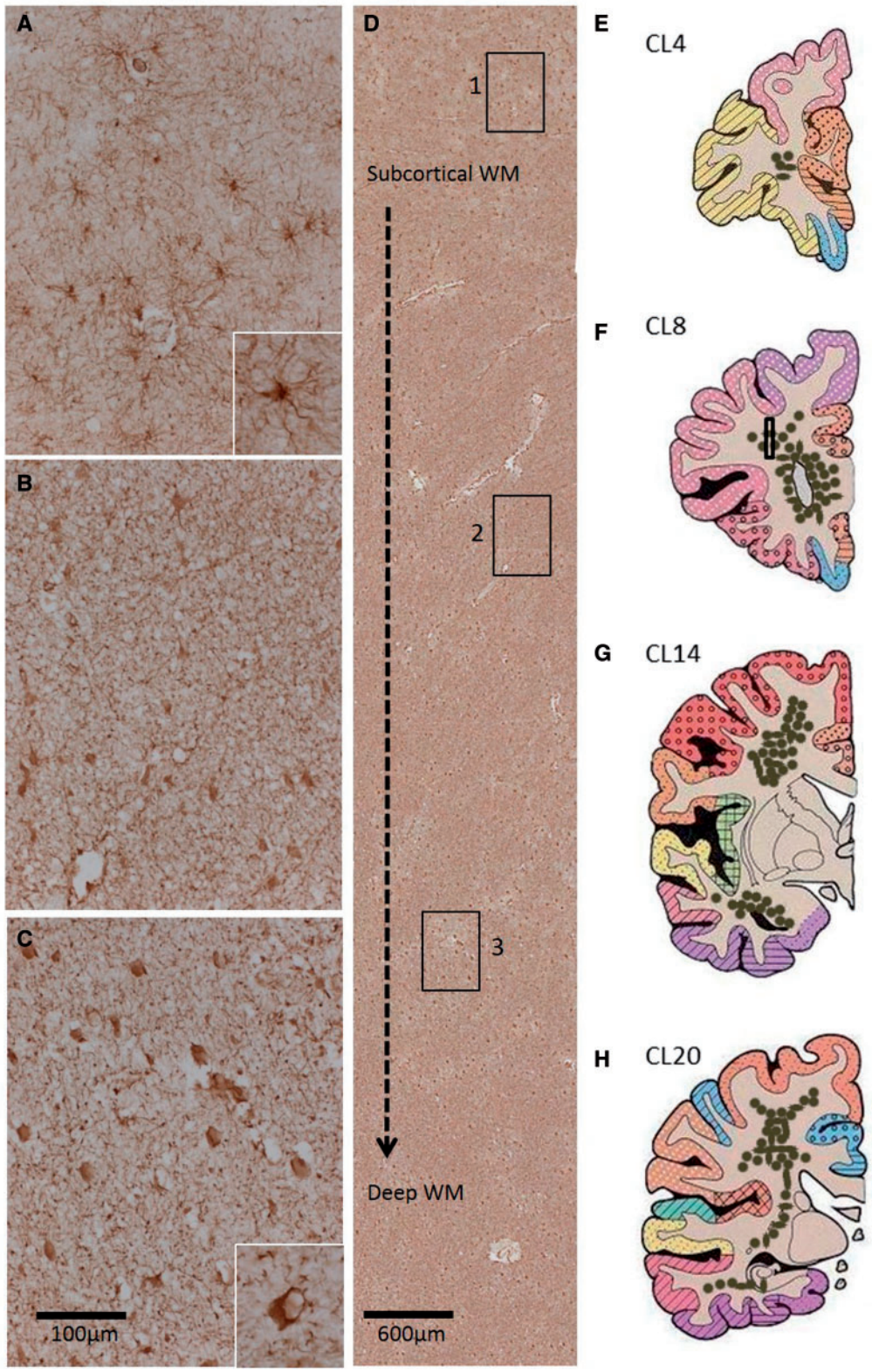

Figure 2 Distribution of GFAP+ clasmatodendrocytes in the deep white matter regions of post-stroke survivors. (**A–C**) Panels show normal appearance of GFAP+ astrocytes in the immediate superficial layers of the white matter (**A**), retracted astrocytes at mid-level (**B**) and clasmatodendrocytes in the deep white matter, with a particularly high concentration at the level of the anterior horn of the lateral ventricles (**C**). Insets in **A** and **C** show a higher magnification of the different forms of GFAP+ astrocytes predominant in **A** and **C**, respectively. In **C** inset, cell vacuolation is evident. Boxes 1–3 in **D** delineate location of images (**A–C**), demonstrating the distribution of GFAP+ cells from the immediate subcortical layer to the deep white matter. Illustrative coronal sections (**E–H**) shows the distribution of clasmatodendrocyte densities (brown dots) in the white matter regions at different coronal levels incorporating the frontal, temporal and parietal lobes. Box in F represents approximate location of image D. Scale bars = 100 μm (**A–C**); 20 μm (insets). WM = white matter.

($\rho = 0.754$, $P < 0.001$). We also showed there was a positive correlation between the frontal and temporal total GFAP immunoreactivities ($\rho = 0.500$, $P = 0.003$) (plots not shown).

For immunofluorescent labelling, the primary antibodies were removed and sections washed with PBS prior to incubation at room temperature for 1 h with goat anti-mouse secondary antibody, Dylight 650 conjugated (1:200, 84545, Thermo Scientific) and goat anti-rabbit secondary antibody, Texas Red conjugated (1:200, T2767, Life Technologies). Sections were counterstained and mounted with DAPI incorporated mounting medium (Dako). A Leica TCS SP2 UV AOBS MP (upright confocal microscope) and a Life Technologies EVOS FL (LED) fluorescent microscope were used for image capture.

White matter rating scale and myelin density

Severity of white matter damage and myelin density was assessed by examining Luxol fast blue and haematoxylin and eosin stained sections using the Zeiss Axioplan 2 research grade microscope at ×5 and ×10 magnification. The myelin index was determined by assessing Luxol fast blue stained sections (Ihara *et al.*, 2010). To achieve this the entire white matter region in 10-µm Luxol fast blue-stained sections of the whole coronal face at the level of Brodmann area (BA) 9 in the frontal lobe and BA 36 in the temporal lobe per Newcastle Brain Reference Map (Perry and Oakley, 1993) was outlined automatically using the wand tool on Image Pro software (Mediacybernetics, USA) as described previously (Ihara *et al.*, 2010). Digital images of the white matter area were then converted to grey scales, corresponding to the staining intensity, from point 0–127 (0, white; 255, black). The intensity profile was then divided into four quartiles (the first quartile 0–29, the second 30–62, the third 63–94, and the fourth 95–127) and the per cent area for each quartile was calculated. The median grey level of each quartile (14.5, 46.0, 78.5, and 111.0), an estimate for the staining intensity, was then multiplied by % area/100 in each quartile, which gave the total myelin index. Highest myelin index value indicates no myelin loss, whilst lowest myelin index indicates total myelin loss and the levels inbetween indicate varying degrees of myelin density. We also verified the degrees of myelin density (normal, mild, moderate and severe) by imaging adjacent haematoxylin and eosin stained sections in a subset of cases ($n = 35$). These data together with accumulation of degraded myelin basic protein showed remarkable consistency in the assessment of myelin loss between Luxol fast blue and haematoxylin and eosin (Sjobeck *et al.*, 2005; Ihara *et al.*, 2010; Smallwood *et al.*, 2012).

The intensity of fibrinogen immunoreactivity across the whole white matter in coronal sections taken from identical levels (equivalent to BA 9 at level of precentral gyrus) from each animal, was determined by ImageJ integrated optical density analysis (Kalaria *et al.*, 2012). The fibrinogen immunoreactivity represented an arbitrary scale determined from the digital images (as above). Images from sham were set at a value of 10 on the scale and all groups were normalized to the sham group.

To assess the degrees of arteriolosclerosis, the sclerotic index (SI) and perivascular spaces were quantified in the white matter of the brains, inclusive of controls. The Vascal programme (Yamamoto *et al.*, 2009) was used to measure the external diameter (Dext) of the vessel and the diameter (Dint) of the lumen. These values were then used to calculate the sclerotic index and perivascular space for each vessel using the equation: SI = 1 − (Dint/Dext).

Cellular morphometry and microvascular markers

For glial cell morphometry, 30-µm thick paraffin sections were stained with cresyl fast violet (Khundakar *et al.*, 2009) and the cell density was determined using the optical dissector method under a Zeiss Axioplan Photomicroscope. Cells in the cortical layers or white matter regions of interest were distinguished by their shape and subtle features (Khundakar *et al.*, 2009). Glial cells were identified by their spherical shape, absence of Nissl staining in the cytoplasm and the heterogenous arrangement of chromatin in the nucleus. Neurons were identified by the presence of a Nissl-stained cytoplasm, pale nucleus and single identifiable nucleolus in cells. The reference area was mapped out using a 2.5 × objective and Visiopharm Integrator System (VIS) software. In pilot studies, we determined that ~40 frames in up to three sections from each case comprising >100 cells per case had to be assessed to reduce the sampling error or the coefficient of error value (defined as the standard error of the mean of repeated estimates divided by the mean) to a satisfactory level, $P < 0.05$ (Burke *et al.*, 2014; Foster *et al.*, 2014).

For the microvascular markers, 20-µm thick serial sections were immunostained with antibodies to GLUT1 (1:200, ThermoScientific UK), a marker for endothelial cells in microvessels. GLUT1 immunostained microvessel profiles were then quantified in whole coronal sections as described previously (Burke *et al.*, 2014). As above, frontal lobe sections were analysed at the level of the olfactory bulbs incorporating BA 9 and the temporal lobe sections at the level of the anterior hippocampus and BA 36 per Newcastle Brain Map (Perry and Oakley, 1993).

Except for the neuropathological examination (by T.M.P and R.K) described above, all of the morphological analyses were always performed under operator blinded conditions. Samples were appropriately identified with coded sequential numbers. We also repeated all staining at least twice and used at least three sections for staining throughout (Foster *et al.*, 2014). In addition, at least two of each positive and negative controls were included to monitor the quality of staining.

Statistical analysis

Statistical analysis was carried out using SPSS Version 21 with the level of significance set at $P < 0.05$. Normal distribution of values was first tested using the Shapiro-Wilk test. In previous analyses, data found to be not normally distributed were analysed using non-parametric methods. Group means such as PSND, PSD and controls were compared using ANOVA with *post hoc* Tukey tests for normal data or Kruskall-Wallis, Newman-Keuls and the Mann-Whitney U-tests for non-normally distributed values e.g. differences between pathological variables and total GFAP+ cells or the ratios of clasmatodendrocytes in different groups.

Spearman's rank ρ correlation was used to assess correlations between clinical and neuropsychometric variables or specific protein immunoreactivity measures and microvascular changes.

To examine the associations between exposure to putative risk factors for dementia, Cox proportional regression analyses were used to obtain univariate proportional hazard ratios for each risk factor, using time (days) from index stroke to dementia as the dependent variable. If a patient died, data were right censored. The date of onset of dementia was assumed to be at the midpoint between the two assessments where dementia status changed. Hazard ratios were given according to presence or absence of the risk factor, or per point on quantitative scales, as appropriate. Following identification in univariate models, frontal white matter hyperintensity volume and other significant predictors of dementia were entered into a multivariate Cox regression model.

Results

Frontal lobe white matter hyperintensity as a predictor of survival to dementia

The frontal lobe white matter hyperintensity volume was determined in 106 subjects scanned during life. Figure 1A shows the survival curves to dementia in non-demented subjects, who remained stable and those who declined to dementia after stroke. Univariate Cox survival analysis for time to dementia indicated volume of white matter hyperintensities was a significant neuroimaging predictor of shorter time to dementia onset (Table 1). The multivariate model controlling for age also showed frontal white matter hyperintensity volume as an independent predictor of survival to dementia [$P = 0.034$, Hazard ratio 95% 1.88 (1.05 to 3.36)], indicating increased white matter hyperintensities volume in those who developed dementia. However, when we included the cognitive scores there was only a trend for the frontal white matter hyperintensity volume to predict survival to dementia (Table 1). Of these post-stroke survivors who had MRI in life, 14 stable (PSND) and decliners, who developed post-stroke dementia (PSD) came to autopsy. Pathological examination showed typical vascular and ischaemic stroke related tissue changes. The total vascular pathology scores between all the PSND and PSD were not significantly different (Table 2).

Frontal lobe white matter astrocytes in post-stroke survivors

To explain the differential findings of the frontal white matter hyperintensity volumes, we attempted identification of markers to delineate the two groups. We hypothesized that reactive cells of the gliomicrovascular unit or myelin are more affected in the frontal white matter of PSD compared to PSND subjects. We first noted that there was increased diffuse fibrinogen immunoreactivity in the frontal white matter in PSD compared to PSND subjects [Fig. 1B(d and h)]. The fibrinogen immunoreactivity in PSD subjects was frequently associated with normal-appearing and rounded astrocytic cells [Fig. 1B(h)]. Using light and fluorescent microscopy, we assessed GFAP+ astrocytes in coronal sections throughout the brain with emphasis on the frontal and temporal white matter. We observed GFAP+ astrocytes of various shapes and sizes (Fig. 2) in both frontal and temporal white matter. As expected 'normal' GFAP+ astrocytes (Fig. 2A) had numerous long, fine processes. However, in the deeper layers of the white matter we noted GFAP+ clasmatodendrotic cells with swollen and vacuolated appearance and many bearing isolated beaded processes (Fig. 2C). Examination of complete coronal sections incorporating the whole of the white matter revealed gradients of normal to clasmatodendrotic astrocytes (Fig. 2D). The deeper layers exhibited many more clasmatodendrocytes than the superficial layers with a high concentration near the ventricles. Mapping of coronal sections (Fig. 2E–H) from the four lobes of PSD and PSND subjects indicated that the highest concentration of clasmatodendrocytes was apparent in the frontal lobe within the deep white matter at the level of the middle frontal gyrus and anterior horn of the lateral ventricles and incorporating the centrum semiovale region. Observations from all the 40 post-stroke brains (Table 2) indicated that the density of clasmatodendrocytes found in the subcortical regions were in following decreasing order: frontal white matter > prefrontal white matter $\geqslant$ temporal white matter $\geqslant$ parietal white matter > lenticular nuclei regions. Clasmatodendrocytes in the external or internal capsules were seldom present.

Quantification of the total GFAP+ cells in the white matter and the percentage of clasmatodendrocytic cells with swollen cell bodies and beaded processes revealed dissimilarities between the PSND and PSD groups and compared to young and older controls (Fig. 3). There were no significant differences between PSND and PSD groups with respect to the total GFAP+ cells in both frontal and temporal deep white matter ($P = 0.850$ and $P = 0.745$, respectively). However, the presence of stroke increased the number of astrocytes as shown by the increased total number of GFAP+ cells in the PSND and PSD groups in the temporal white matter compared to the similar age controls (Fig. 3A; $P = 0.007$ and $P = 0.018$, respectively). We also found an ageing effect in that the older controls had fewer astrocytes in both the frontal ($P = 0.04$) and temporal white matter ($P = 0.007$) compared to younger controls (Fig. 3A). These changes were restricted to the frontal white matter rather than the grey matter. The 3D morphometric analyses showed that glial cell density in the neocortex (layers III and V) was not changed between PSND and PSD subjects ($P > 0.05$). There was also paucity of clasmatodendrosis in the neocortex.

Most remarkably, we observed that the percentage of clasmatodendrocytes in the frontal white matter was

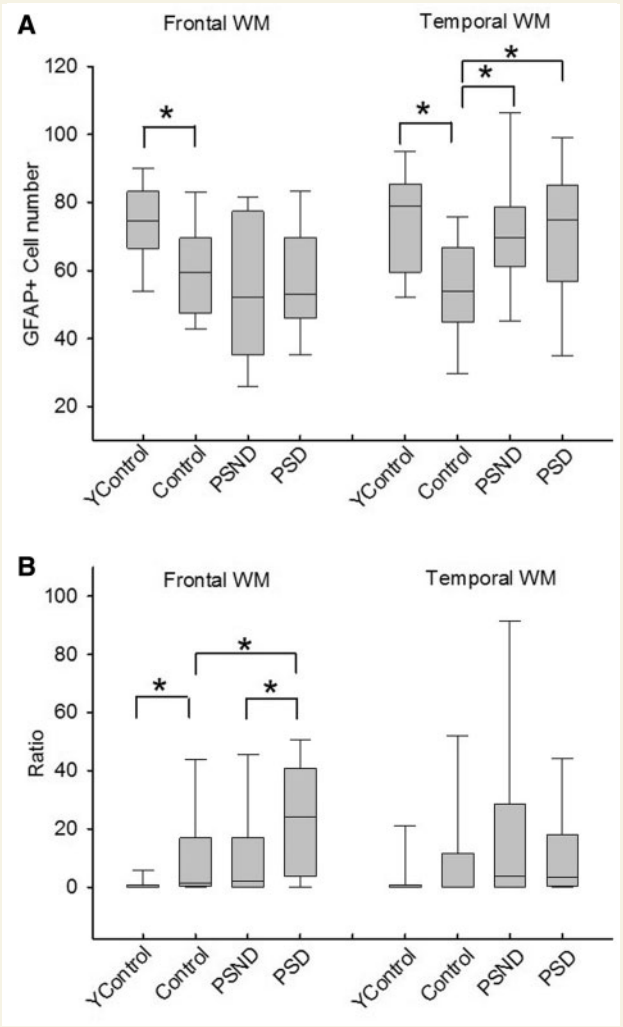

Figure 3 Quantification of GFAP+ cell numbers in the frontal and temporal white matter in controls, PSND and PSD subjects. (**A**) Box plots show total GFAP+ astrocytes in the frontal and temporal white matter. (**B**) Box plots show ratios of the number of clasmatodendrocytes to total cells in the two white matter regions. The *y*-axis values are × 100. Number of samples for each group are given in Table 2. The analysis was performed in duplicate and gave similar results. *Significance: frontal white matter total GFAP, young Control versus Control $P = 0.04$; temporal white matter total GFAP, young Control versus Control $P = 0.007$, Control versus PSND $P = 0.007$, Control versus PSND $P = 0.018$; frontal white matter ratios GFAP, young Control versus Control $P = 0.023$, Control versus PSD $P = 0.033$, PSND versus PSD $P = 0.03$. (Mann-Whitney U-test) between the groups. Ycontrol = young controls. Control represents age-matched subjects to all groups except young controls. WM = white matter.

significantly greater (by 100%) in the PSD than in the PSND group (Fig. 3B; median = 0.24 for PSD, median = 0.02 for PSND, $P = 0.030$), but a similar increase was not evident in the temporal white matter (median = 0.03 for PSD and 0.04 for PSND, $P = 0.725$). In comparison with older age-matched controls (median = 0.015 and 0.002 for frontal and temporal white matter, respectively), there was more clasmatodendrosis in the frontal white matter of PSD ($P = 0.082$), which was not apparent in the PSND group (Fig. 3B). We also found a striking difference between older and younger controls ($P = 0.023$), with almost no presence of clasmatodendrocytes in either the frontal or temporal white matter in young controls. Multiple regression analysis for dependent variable (parameter from cognitive test), with independent variables (age, frontal or temporal white matter GFAP + cell numbers, ratio of clasmatodendrosis) performed for PSND and PSD patients, showed weak inverse correlations with various cognitive function tests including MMSE ($\rho = 0.355$, $P = 0.024$), CAMCOG ($\rho = 0.348$, $P = 0.028$) and total memory ($\rho = 0.338$, $P = 0.033$) scores as a function of age.

To exclude possible post-mortem effects on the occurrence of clasmatodendrosis, subjects with mild (<10%) and severe (≥10%) clasmatodendrosis were divided into two separate groups. There were no statistical differences in post-mortem delay (h) between cases with mild and severe clasmatodendrosis (Supplementary Table 1). There were more cases with severe clasmatodendrosis in the PSD group than in the PSND and control groups. In addition, the presence of clasmatodendrosis was not related to tissue fixation time or with the age or gender of the subjects.

Double immunofluorescent staining showed co-localization of GFAP and AQP4 in astrocytes (Fig. 4). In the areas with normal GFAP staining, AQP4 displayed an evenly distributed pattern with punctate reactivity within the astrocytic end-feet. In areas of clasmatodendrosis, AQP4 was aggregated in dense peripheral cellular deposits at the edge of rounded or swollen GFAP+ cells (Fig. 4A). We also noted transitional forms of GFAP+ cells or astrocytes where they exhibited reduced processes and cell body swelling (Fig. 4A). The disintegration of the GFAP+ cells was further evident in astrocytes immunolabelled with ALDH1L1 antibodies. ALDH1L1 as a cytoplasmic marker showed the differential disintegration of the clasmatodendrocytes. The cytoplasmic structure was disrupted in more cells with soma vacuolation in contrast to the remnant GFAP immunoreactivity in cytoskeletal proteins (Fig. 4B). In subsequent experiments, we showed that clasmatodendrocytes were also immunoreactive for another marker, DLL1, which labelled most astrocytes. Consistent with the autophagic mode of cell death, we found that clasmatodendrocytes expressed PARP1 and LC3 immunoreactivities (Supplementary Fig. 1).

We further showed that the white matter microvessel or capillaries were denuded of AQP4 immunoreactive astrocytic end-feet. This was readily seen in sections double immunolabelled with AQP4 and COL4, particularly in the PSD cases (Fig. 5). We noted that numerous capillaries exhibited absence of astrocytic end-feet that was most conspicuous in areas of fibrinogen immunoreactivity in subjects with PSD.

In additional experiments, we also found that white matter damage severity score correlated positively with the vascular

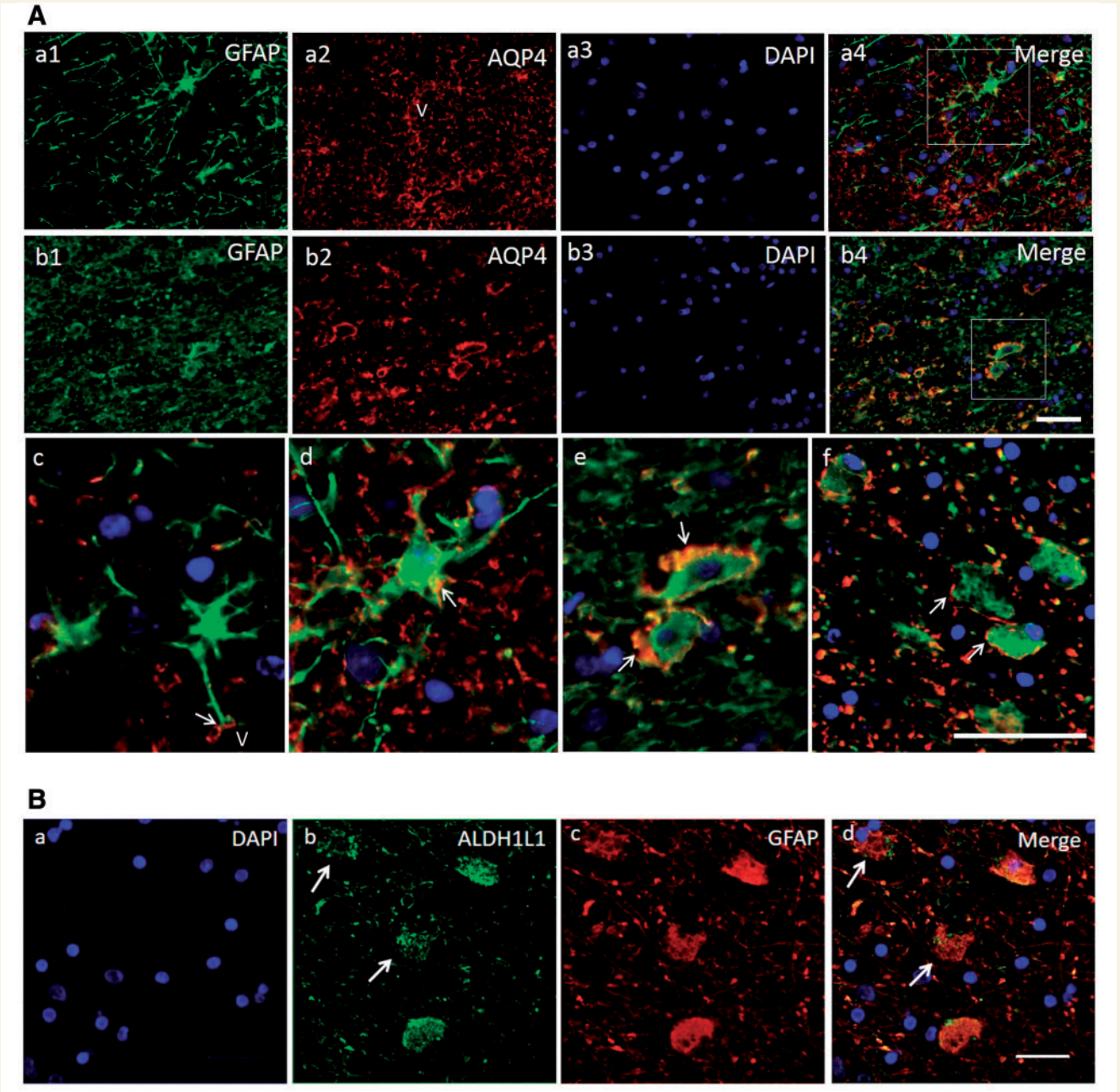

Figure 4 Transformation of GFAP+ cells in the deep white matter in relation to microvessels. (**A**) Triple immunofluorescent staining of GFAP (Cy5, Dylight 650 shown in green), AQP4 (Texas Red, shown in red) and DAPI for astrocytes and their processes. **A(a1–4)** is from a PSND case; **A**(**b1–4**) is from a PSD case. **A**(**c**) AQP4 staining is mainly in the end-feet of astrocytes, frequently outlining a vessel (V). **A**(**d**) shows an astrocyte with intermediate level of pathology: AQP4 immunostaining is also seen along the process and in the cellular membrane (white arrow). **A**(**d**) Area outlined in a4. **A**(**e**) Higher magnification of area outlined in **b4**, demonstrates AQP4 is aggregated in dense peripheral cellular deposits, at the periphery of the GFAP stained swollen astrocyte. **A**(**f**) Another example of astrocytes with GFAP stained swollen bodies and fragmented processes, and demonstrates that AQP4 is located at the edge of cell bodies of retracted astrocytes (white arrows). **A**(**d–f**) The progressive degenerative change or transition of the astrocytes. DAPI was used for nuclear counterstaining, which is eventually lost from the astrocytes. (**B**) GFAP and ALDH1L1 immunoreactivities in clasmatodendrocytes in the deep white matter in a PSD subject. **B**(**a–d**) Clasmatodendrocytes representing degenerating GFAP+ cells (arrows in **b**) lacking cytoplasmic ALDH1L1 reactivity. Scale bars in **A** (both in **b4** and **f**) = 20 μm and in **B** = 25 μm.

score ($\rho = 0.674$, $P < 0.001$) but inversely with the myelin index ($\rho = -0.750$, $P < 0.001$). Higher myelin index meant better preserved myelin, as the index in this context is a measure of normal myelin (Ihara *et al.*, 2010). The myelin index was relatively higher in the control compared to PSND and PSD groups in the frontal white matter, and the variation showed a trend towards significance ($P = 0.069$, Kruskal–Wallis Test). The difference in myelin index between controls

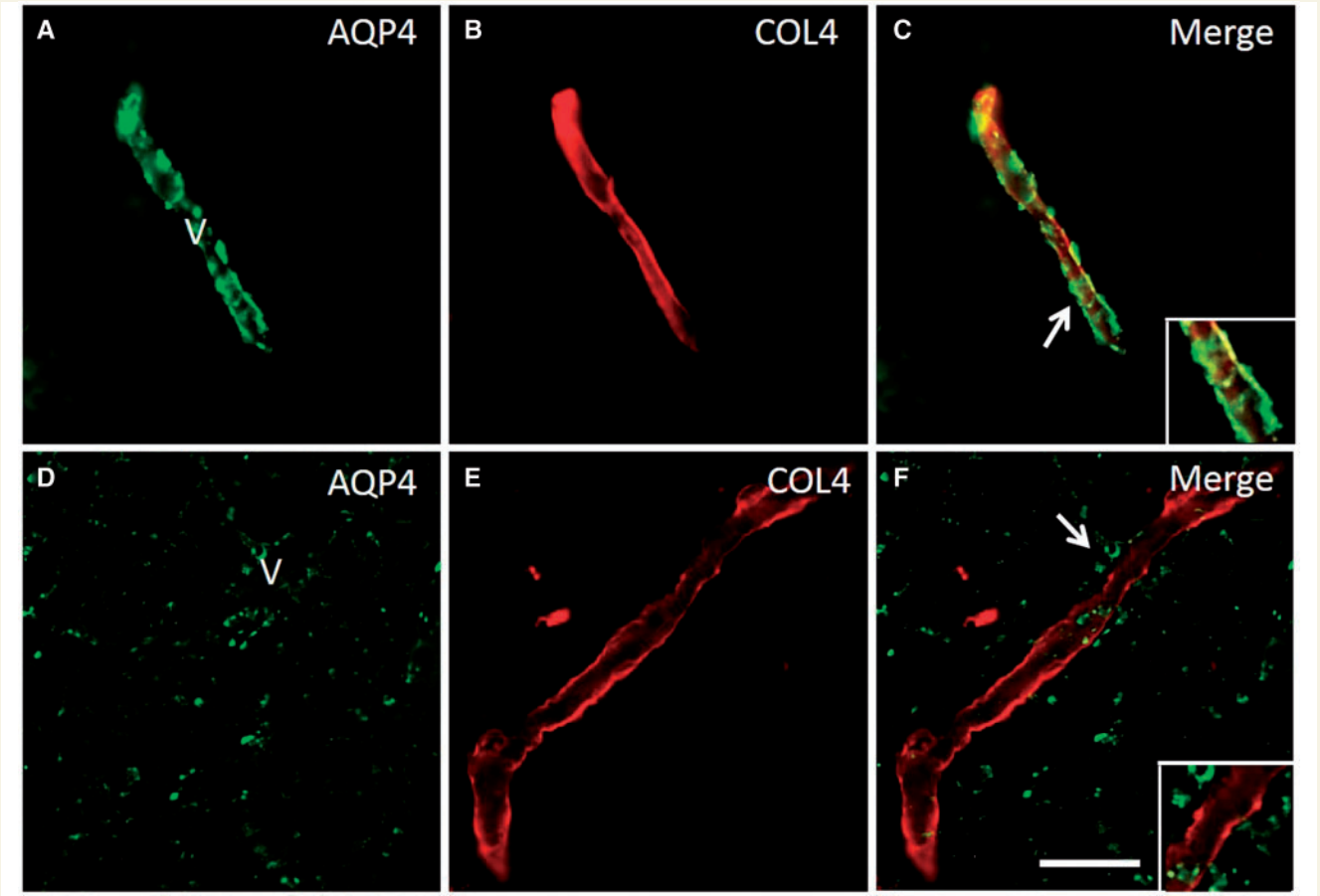

Figure 5 Redistribution of AQP4 from COL4 labelled microvessels and capillaries in the deep white matter in PSD. (**A–C**) Panels show a AQP4 and COL4 labelled capillary in deep white matter of a PSND case demonstrating localization of AQP4 immunoreactivity in the vessel wall (**C**). (**D–F** and insets) show lack of co-localization of AQP4 and COL4 in regions where clasmatodendrocytes were found. The disrupted distribution of AQP4 is evident in **F** (arrow). Scale bar = 25 μm.

and the pathological groups (PSND, PSD) was surprisingly lower than expected in both frontal and temporal white matter, possibly due to a significant amount of white matter disease in the control group.

Blood–brain barrier integrity and presence of clasmatodendrocytes in frontal white matter in a non-human primate model

To demonstrate that the phenomenon of clasmatodendrosis occurring in white matter was associated with blood–brain barrier changes and not a consequence of antemortem or post-mortem modification within the brain tissue, sections from baboons subjected to cerebral hypoperfusion by three-vessel occlusion were immunolabelled with antibodies to fibrinogen, GFAP and AQP4 (Fig. 6). In these series of experiments, we first quantified fibrinogen immunoreactivity in the frontal white matter incorporating the equivalent region of interest as in the PSD subjects. Analysis at different periods of survival after three-vessel occlusion showed that the greatest amount of fibrinogen immunoreactivity was evident in 14-day animals. Fibrinogen immunoreactivity was significantly increased at 14 days compared to animals that survived 1 day after the occlusion as well as the sham operated animals (Fig. 6A). These observations were consistent with the development of severe white matter changes at 14 days after three-vessel occlusion, predominantly in the deep white matter (Supplementary Fig. 2). Using double immunofluorescent methods as with human post-mortem tissue (Fig. 6B), we analysed a series of adjacent coronal sections from the baboon brains. In the 14 day animals, remarkably we found similar distribution of GFAP+ clasmatodendrocytes with the characteristic AQP4 immunoreactivity at the edge of the retracted cell bodies (Fig. 6B). This phenomenon was not evident in the sham or 1 day animals and as in human cases, there were no apparent white matter infarcts or ischaemic lesions in the vicinity of the clasmatodendrocytes. Furthermore, the white matter changes were associated with myelin loss, collapsed and degenerated microvessels

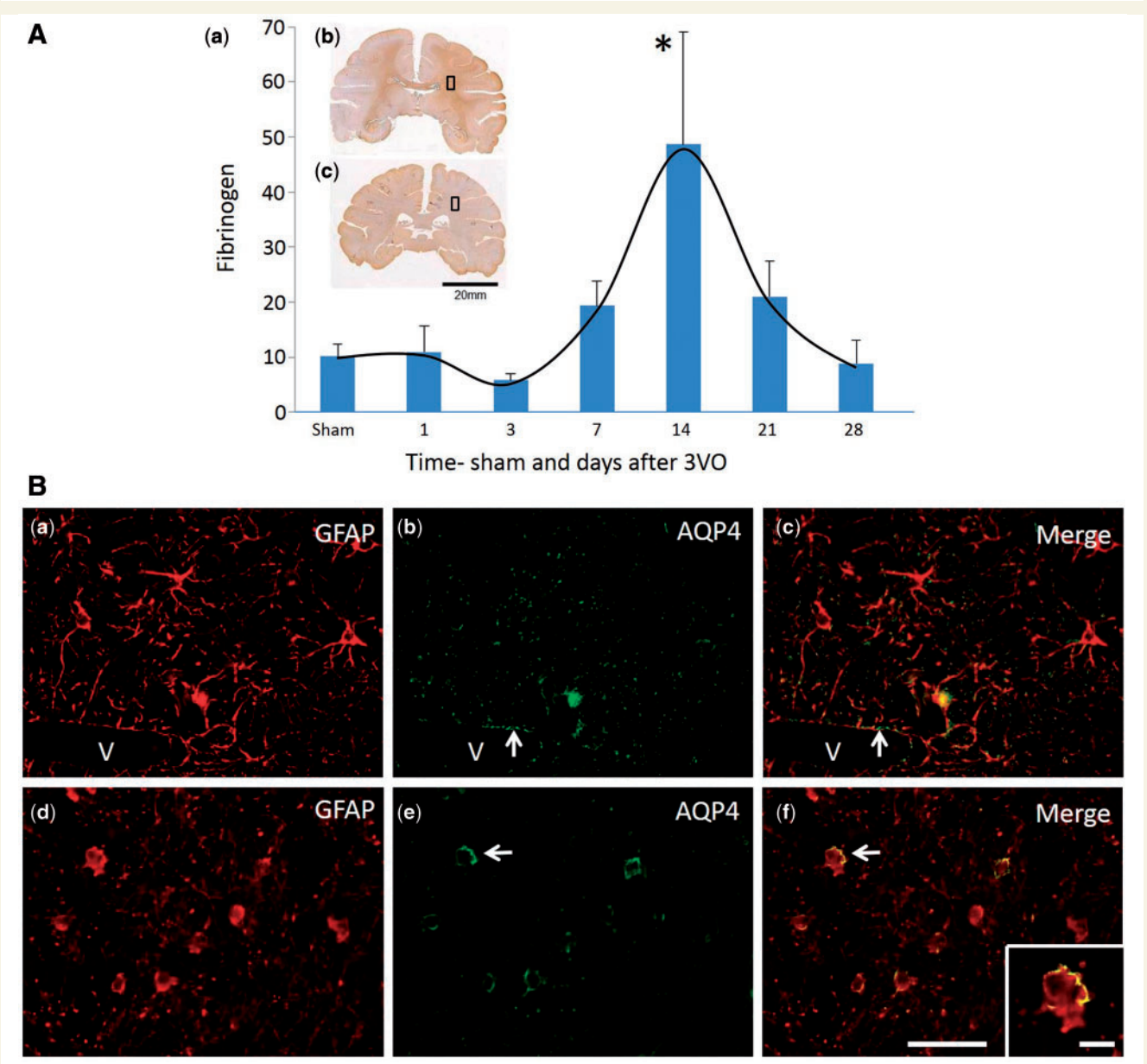

Figure 6 Integrity of the blood–brain barrier and presence of clasmatodendrocytes in the frontal white matter in a non-human primate model of cerebral hypoperfusion. [**A**(**a**)] Quantification of fibrinogen reactivity in the frontal white matter of adult baboons subjected to three-vessel occlusion (3VO). Brain images [**A**(**b** and **c**)] within the graph show the approximate coronal level of sampling for immunofluorescent staining. Each time point denotes the mean level of fibrinogen from $n = 4–7$ animals and these results were obtained from both hemispheres. There were no differences between the right and left hemispheres. ANOVA showed that there was a high variation in fibrinogen immunoreactivity across all time points ($P < 0.01$). *Significance $P < 0.05$ compared to 1 day and sham groups. [**B**(**a–c**)] Astrocytes from the frontal white matter of a sham animal, demonstrating normal distribution of GFAP [**B**(**a**)] and AQP4 [**B**(**b**)], with no sign of abnormalities. **B**(**c**) is the merged image of **B**(**a** and **b**). Arrows denote AQP4 around periphery of blood vessel (V). [**B**(**d–f**)] Astrocytes in white matter of an animal after 14 days of three-vessel occlusion, demonstrating clasmatodendrosis of the astrocytes immunolabelled with GFAP [**B**(**d**)] and an abnormal distribution of AQP4 [**B**(**e**)]. **B**(**f**) A merged image of **B**(**d** and **e**). The inset shows high magnification of a clasmatodendrocyte identified in **B**(**f**) (arrow) with typical peripheral distribution of AQP4 on the cell body. Scale bar = 50 μm; inset (**f**) = 20 μm.

labelled with endothelial (GLUT1) and basement membrane (COL4) markers at 14 days after three-vessel occlusion (Supplementary Fig. 3). The subsequent reduction in fibrinogen immunoreactivity and the lack of clasmatodendrocytes (Fig. 6) together with increases in immunoreactivities of the GLUT1 and COL4 in capillaries within the frontal white matter beyond 14 days were consistent with recovery of the patency or the reconstruction of

the microvasculature to establish tissue perfusion (Supplementary Fig. 3).

Discussion

Our study provides strong evidence for another pathological substrate which contributes to the development of dementia in post-stroke survivors, most of whom had vascular dementia. We found highly increased degeneration of astrocytes in PSD subjects who had greater more confluent white matter hyperintensities volumes. Clasmatodendrosis was particularly prominent in the deep white matter of the frontal lobe. Whereas markers of both myelin and axon damage including the myelin index and immunoreactivities of degenerated myelin basic protein, amyloid precursor protein and SMI32 in the white matter (Akinyemi, 2014; Foster *et al*., 2014) tended to be increased in the PSD compared to the PSND subjects, quantification of clasmatodendrosis clearly separated the post-stroke stable from those who developed dementia. The experimental design of the study also allowed us to demonstrate that the observed clasmatodendrosis was not necessarily associated with peri-infarct regions (as we avoided these) but largely within the deep white matter undergoing rarefaction both in human and non-human primate brains. Our findings suggest that clasmatodendrosis is a pathological gauge for disruption of gliovascular interactions (Abbott *et al*., 2006) likely instigated by underlying blood–brain barrier abnormalities in the deep white matter of the frontal lobe. We propose that this is an important factor, which explains the association between white matter hyperintensities and cognitive dysfunction in stroke survivors, cerebral small vessel disease and vascular dementia. The findings are consistent with previous observational studies indicating the presence of clasmatodendrosis in dementing disorders with white matter pathology (Tomimoto *et al*., 1996; Sahlas *et al*., 2002).

Clasmatodendrosis may occur during different conditions. Both neuromyelitis optica and central pontine myelinolysis are primary astrocytopathies with secondary demyelination. Clasmatodendrosis in the absence of demyelination or axonal degeneration is one of the six different lesion types described in neuromyelitis optica (Misu *et al*., 2013). Another type occurs with a variable degree of astrocyte clasmatodendrosis, plaque-like primary demyelination and preservation of axons. These different types of lesions may indicate how the pathology progresses or be a pathological change accompanying other diseases, such as in ischaemic stroke. In acute haemorrhagic leukoencephalitis (Robinson *et al*., 2014), there was early and widespread astrocytic injury with swollen cell bodies and beaded processes in the absence of demyelination, suggesting that demyelination is secondary to astrocyte injury, similar to that in neuromyelitis optica and central pontine myelinolysis (Misu *et al*., 2013; Popescu *et al*., 2013; Lucchinetti *et al*., 2014).

We also found that although the total astrocyte population in the frontal white matter was decreased, the numbers of clasmatodendrocytes were increased in older age. This is consistent with the fact that age *per se* is an important contributor to the progression of white matter pathology during brain ageing and relates to the increased white matter hyperintensity volume (Inzitari *et al*., 2009).

The frontal white matter was more affected than the temporal white matter in PSD patients, which possibly relates to the frontal lobe being more vulnerable in cerebrovascular disease. Previous imaging and pathological studies have suggested that the medullary arteries and white matter in the frontal lobe are particularly susceptible to a haemodynamic derangement, leading to much more severe white matter damage than in the temporal lobe, during ageing and vascular disease (Furuta *et al*., 1991; Ihara *et al*., 2010). Tomimoto *et al.* (1996) demonstrated that there is significantly more fibrinogen and immunoglobulins in brains containing clasmatodendrosis than in brains without, which suggested dysfunction of the blood–brain barrier. In addition, the reduction of cerebral blood flow and cerebral perfusion was suggested to contribute to cognitive impairment in chronic stroke patients (Mori *et al*., 1994). We previously reported the association between the global cerebral blood flow in the grey matter/white matter ratio and PSD (Firbank *et al*., 2011) and it is plausible that blood flow is a direct cause of clasmatodendrosis (Kraig and Chesler, 1990; Qin *et al*., 2010).

Variations in clasmatodendrosis may also be influenced by various factors. The degree of clasmatodendrosis increased from the immediate subcortical layers toward the deep white matter region, which may be due to a staged response, possibly in relation to disease duration or severity, or possibly a mixture of both. The differing areas of clasmatodendrosis in patients suggests the variation in the extent of the stroke or a different response to remote stroke lesions (Allan *et al*., 2011). Factors, such as previous symptomatic stroke, previous asymptomatic stroke seen on imaging, recurrent stroke, several stroke lesions, volume of the infarct and location of stroke, were also associated with PSD (Pendlebury and Rothwell, 2009). However, the experimental evidence showed that clasmatodendrosis occurs rather acutely after induction of cerebral hypoperfusion in non-human primates suggesting that recurrent changes in perfusion pressure may constantly disrupt gliovascular interactions, which progressively worsen with ageing. Clasmatodendrosis of astrocytes can occur due to a drop in tissue pH irrespective of the presence of glycolysis (Friede and van Houten, 1961). Therefore, it is necessary to distinguish normal tissue glycolysis from any antemortem or post-mortem effects. We found no differences in the post-mortem delay times between samples with mild and severe clasmatodendrosis, suggesting the difference in the severity of clasmatodendrosis between PSND and PSD was an actual representation of astrocyte pathology. Furthermore, experimental evidence from perfused fixed baboon brains showed that similar clasmatodendrosis

was associated with blood–brain barrier protein leakage and abnormalities in the microvascular endothelium resulting from cerebral hypoperfusion. Furthermore, our findings here are entirely consistent with the association of gliovascular alterations and cognitive deficits we reported earlier (Holland *et al.*, 2015) in a mouse model of sustained cerebral hypoperfusion with features of small vessel disease (white matter disruption) induced by bilateral common carotid stenosis (BCAS) (Okamoto *et al.*, 2012). In our BCAS model, we showed that gliovascular changes revealed a marked increase in microvessel diameter, vascular wall disruption, fibrinoid necrosis, haemorrhage, and blood–brain barrier alterations with widespread reactive gliosis, including displacement of the astrocytic water channel, AQP4 (Holland *et al.*, 2015). The gliovascular changes reported in this model were more pronounced in the subcortical thalamic regions but similar alterations occured in the corpus callosum. Such spatial dissociation between the vascular basement membrane and the astrocyte endfeet also occurs in ischaemic brain in spontaneously hypertensive rats with middle cerebral artery occlusion (MCAO) (Yamashita *et al.*, 2009). The basement membrane/extracellular matrix linking the endothelial cells appear essential for maintaining the integrity of the neuro- or gliovascular unit, which is disrupted by tissue plasminogen activator treatment.

The altered AQP4 distribution in the shrinking processes and the swelling of astrocytic cell bodies relates to changes in water mobility or the disturbance of water homeostasis (Taniguchi *et al.*, 2000). It may also affect the local microcirculation, since AQP4 is located predominantly at the end foot and ependyma of astrocytes, which wrap around brain microvessels (Badaut *et al.*, 2002). AQP4 provides structural integrity to the cerebral vasculature (El-Khoury *et al.*, 2006) and also promotes water exchange between blood and CSF in pathophysiological conditions. The occurrence of clasmatodendrosis in Alzheimer's disease combined with cerebrovascular disease but not in Alzheimer's disease without vascular pathology (Tomimoto *et al.*, 1996), indicates an involvement of vascular events in the onset of clasmatodendrosis. It is expected that astrocyte pathology is differentially involved in Alzheimer's disease, vascular dementia and mixed (Alzheimer's disease and vascular dementia) subjects and the severity of clasmatodendrosis may depend on the extent of cerebrovascular pathology in these diseases.

Are astrocytes an early target before neuronal or axonal damage in ischaemic injury? Astrocyte cultures from the hippocampus (Hulse *et al.*, 2001), after exposure to acidic Ringer's solution and mitochondrial inhibition, showed that the greatest degree of clasmatodendrosis occurred in the pyramidal cell body layers and closely paralleled that seen *in vivo* (Friede and van Houten, 1961). Given these observations, we cannot rule out that low level clasmatodendrosis occurs in the pyramidal cell layers of the cortex above the white matter in our cases and together with white matter astrocyte pathology could directly or indirectly causes neuronal damage, resulting in cognitive dysfunction (Gemmell *et al.*, 2012; Foster *et al.*, 2014).

We have provided clinical, pathological and experimental evidence to support the interpretation of our findings on how cognitive function in ageing subjects with greater volumes of white matter hyperintensities may decline. However, there are some limitations of the study. We could not provide pathological data from all the post-stroke survivors who had MRI in life but were only able to analyse a sizeable sample as a proxy. We were also limited in assessing blood–brain barrier or perfusion changes in the white matter *in vivo* (Wardlaw *et al.*, 2009) to complement the pathological findings and show directly that frontal lobe white matter perfusion is more vulnerable in post-stroke survivors or those subjects with cerebral small vessel disease who decline cognitively to develop dementia.

In summary, our findings suggest a novel association between the irreversible astrocyte injury (clasmatodendrosis) and PSD. This large aetiological study of clasmatodendrosis after stroke enables us to understand more about the pathophysiological substrates associated with brain ageing, PSD and vascular dementia. The information gained may also be invaluable in producing interventions to reduce the rate of clasmatodendrosis, which in turn could help to reduce the burden of dementia.

Acknowledgements

We are grateful to the patients, families, and clinical house staff for their cooperation in the investigation of this study. We thank Michelle Widdrington, Carein Todd, Jean Scott, Deborah Lett, and Anne Nicholson for assistance in managing and screening the cohort. We thank Janet Y. Slade and Roslyn Hall for excellent technical assistance. We are most grateful to Katri Tuomela (Linköping University, Sweden) and Deborah Cook (Newcastle University) for generating some of the initial data while undertaking undergraduate research projects.

Funding

Our work is supported by grants from the Dunhill Medical Trust UK (R277/0213), Medical Research Council (MRC, G0500247), Newcastle Centre for Brain Ageing and Vitality (BBSRC, EPSRC, ESRC and MRC, LLHW), and Alzheimer's Research (ARUK). The CogFAST study was originally supported by the MRC in 1999. Tissue for this study was collected by the Newcastle Brain Tissue Resource, which is funded in part by a grant from the UK MRC (G0400074), by the Newcastle NIHR Biomedical Research Centre in Ageing and Age Related Diseases award to the Newcastle upon Tyne Hospitals NHS Foundation Trust, and by a grant from the

Alzheimer's Society and ART as part of the Brains for Dementia Research Project. Rufus O. Akinyemi was supported by a Research Fellowship from the International Brain Research Organization (IBRO) and an Overseas Research Student Award from Newcastle University. Y.H. was supported by the SENSHIN Medical Research Foundation, Osaka, Japan and The Great Britain Sasakawa Foundation, London, UK.

Supplementary material

Supplementary material is available at *Brain* online.

References

Abbott NJ, Ronnback L, Hansson E. Astrocyte-endothelial interactions at the blood-brain barrier. Nat Rev Neurosci 2006; 7: 41–53.

Akinyemi RO. Profile, determinants and mechanisms of cerebral injury and cognitive impairment following stroke. Institute of Neuroscience. Vol PhD thesis. Newcastle upon Tyne: Newcastle University, 2014. p. 280.

Allan LM, Rowan EN, Firbank MJ, Thomas AJ, Parry SW, Polvikoski TM, et al. Long term incidence of dementia, predictors of mortality and pathological diagnosis in older stroke survivors. Brain 2011; 134: 3716–27.

Badaut J, Lasbennes F, Magistretti PJ, Regli L. Aquaporins in brain: distribution, physiology, and pathophysiology. J Cereb Blood Flow Metab 2002; 22: 367–78.

Barker R, Ashby EL, Wellington D, Barrow VM, Palmer JC, Kehoe PG, et al. Pathophysiology of white matter perfusion in Alzheimer's disease and vascular dementia. Brain 2014; 137: 1524–32.

Barker R, Wellington D, Esiri MM, Love S. Assessing white matter ischemic damage in dementia patients by measurement of myelin proteins. J Cereb Blood Flow Metab 2013; 33: 1050–7.

Bolandzadeh N, Davis JC, Tam R, Handy TC, Liu-Ambrose T. The association between cognitive function and white matter lesion location in older adults: a systematic review. BMC Neurol 2012; 12: 126.

Burke MJ, Nelson L, Slade JY, Oakley AE, Khundakar AA, Kalaria RN. Morphometry of the hippocampal microvasculature in post-stroke and age-related dementias. Neuropathol Appl Neurobiol 2014; 40: 284–95.

Burton EJ, Kenny RA, O'Brien J, Stephens S, Bradbury M, Rowan E, et al. White matter hyperintensities are associated with impairment of memory, attention, and global cognitive performance in older stroke patients. Stroke 2004; 35: 1270–5.

de Leeuw FE, de Groot JC, Achten E, Oudkerk M, Ramos LM, Heijboer R, et al. Prevalence of cerebral white matter lesions in elderly people: a population based magnetic resonance imaging study. The Rotterdam Scan Study. J Neurol Neurosurg Psychiatry 2001; 70: 9–14.

Debette S, Markus HS. The clinical importance of white matter hyperintensities on brain magnetic resonance imaging: systematic review and meta-analysis. Br Med J 2010; 341: c3666.

DeCarli C, Murphy DG, Tranh M, Grady CL, Haxby JV, Gillette JA, et al. The effect of white matter hyperintensity volume on brain structure, cognitive performance, and cerebral metabolism of glucose in 51 healthy adults. Neurology 1995; 45: 2077–84.

Deramecourt V, Slade JY, Oakley AE, Perry RH, Ince PG, Maurage CA, et al. Staging and natural history of cerebrovascular pathology in dementia. Neurology 2012; 78: 1043–50.

El-Khoury N, Braun A, Hu F, Pandey M, Nedergaard M, Lagamma EF, et al. Astrocyte end-feet in germinal matrix, cerebral cortex, and white matter in developing infants. Pediatr Res 2006; 59: 673–9.

Firbank MJ, Allan LM, Burton EJ, Barber R, O'Brien JT, Kalaria RN. Neuroimaging predictors of death and dementia in a cohort of older stroke survivors. J Neurol Neurosurg Psychiatry 2012; 83: 263–7.

Firbank MJ, He J, Blamire AM, Singh B, Danson P, Kalaria RN, et al. Cerebral blood flow by arterial spin labeling in poststroke dementia. Neurology 2011; 76: 1478–84.

Foster V, Oakley AE, Slade JY, Hall R, Polvikoski TM, Burke M, et al. Pyramidal neurons of the prefrontal cortex in post-stroke, vascular and other ageing-related dementias. Brain 2014; 137 (Pt 9): 2509–21.

Friede RL, van Houten WH. Relations between post-mortem alterations and glycolytic metabolism in the brain. Exp Neurol 1961; 4: 197–204.

Funfschilling U, Supplie LM, Mahad D, Boretius S, Saab AS, Edgar J, et al. Glycolytic oligodendrocytes maintain myelin and long-term axonal integrity. Nature 2012; 485: 517–21.

Furuta A, Ishii N, Nishihara Y, Horie A. Medullary arteries in aging and dementia. Stroke 1991; 22: 442–6.

Gelot A, Villapol S, Billette de Villemeur T, Renolleau S, Charriaut-Marlangue C. Astrocytic demise in the developing rat and human brain after hypoxic-ischemic damage. Dev Neurosci 2009; 31: 459–70.

Gemmell E, Bosomworth H, Allan L, Hall R, Khundakar A, Oakley AE, et al. Hippocampal neuronal atrophy and cognitive function in delayed poststroke and aging-related dementias. Stroke 2012; 43: 808–14.

Hinson SR, Pittock SJ, Lucchinetti CF, Roemer SF, Fryer JP, Kryzer TJ, et al. Pathogenic potential of IgG binding to water channel extracellular domain in neuromyelitis optica. Neurology 2007; 69: 2221–31.

Holland PR, Searcy JL, Salvadores N, Scullion G, Chen G, Lawson G, et al. Gliovascular disruption and cognitive deficits in a mouse model with features of small vessel disease. J Cereb Blood Flow Metab 2015; 35: 1005–14. doi: 10.1038/jcbfm.2015.12.

Hulse RE, Winterfield J, Kunkler PE, Kraig RP. Astrocytic clasmatodendrosis in hippocampal organ culture. Glia 2001; 33: 169–79.

Ihara M, Polvikoski TM, Hall R, Slade JY, Perry RH, Oakley AE, et al. Quantification of myelin loss in frontal lobe white matter in vascular dementia, Alzheimer's disease, and dementia with Lewy bodies. Acta Neuropathol 2010; 119: 579–89.

Inzitari D, Pracucci G, Poggesi A, Carlucci G, Barkhof F, Chabriat H, et al. Changes in white matter as determinant of global functional decline in older independent outpatients: three year follow-up of LADIS (leukoaraiosis and disability) study cohort. Br Med J 2009; 339: b2477.

Kalaria RN, Ihara M. Dementia: vascular and neurodegenerative pathways-will they meet? Nat Rev Neurol 2013; 9: 487–8.

Kalaria RN, Kenny RA, Ballard CG, Perry R, Ince P, Polvikoski T. Towards defining the neuropathological substrates of vascular dementia. J Neurol Sci 2004; 226: 75–80.

Kalaria RN, Perry RH, O'Brien J, Jaros E. Atheromatous disease in small intracerebral vessels, microinfarcts and dementia. Neuropathol Appl Neurobiol 2012; 38: 505–8.

Khundakar A, Morris C, Oakley A, McMeekin W, Thomas AJ. Morphometric analysis of neuronal and glial cell pathology in the dorsolateral prefrontal cortex in late-life depression. Br J Psychiatry 2009; 195: 163–9.

Kim JE, Ryu HJ, Yeo SI, Kang TC. P2X7 receptor differentially modulates astroglial apoptosis and clasmatodendrosis in the rat brain following status epilepticus. Hippocampus 2011; 21: 1318–33.

Kraig RP, Chesler M. Astrocytic acidosis in hyperglycemic and complete ischemia. J Cereb Blood Flow Metab 1990; 10: 104–114.

Lace G, Savva GM, Forster G, de Silva R, Brayne C, Matthews FE, et al. Hippocampal tau pathology is related to neuroanatomical

connections: an ageing population-based study. Brain 2009; 132: 1324–34.
Lucchinetti CF, Guo Y, Popescu BF, Fujihara K, Itoyama Y, Misu T. The pathology of an autoimmune astrocytopathy: lessons learned from neuromyelitis optica. Brain Pathol 2014; 24: 83–97.
Misu T, Hoftberger R, Fujihara K, Wimmer I, Takai Y, Nishiyama S, et al. Presence of six different lesion types suggests diverse mechanisms of tissue injury in neuromyelitis optica. Acta Neuropathol 2013; 125: 815–27.
Mori S, Sadoshima S, Ibayashi S, Lino K, Fujishima M. Relation of cerebral blood flow to motor and cognitive functions in chronic stroke patients. Stroke 1994; 25: 309–17.
Ndung'u M, Hartig W, Wegner F, Mwenda JM, Low RW, Akinyemi RO, et al. Cerebral amyloid beta(42) deposits and microvascular pathology in ageing baboons. Neuropathol Appl Neurobiol 2012; 38: 487–99.
Okamoto Y, Yamamoto T, Kalaria RN, Senzaki H, Maki T, Hase Y, et al. Cerebral hypoperfusion accelerates cerebral amyloid angiopathy and promotes cortical microinfarcts. Acta Neuropathol 2012; 123: 381–94.
Pendlebury ST, Rothwell PM. Prevalence, incidence, and factors associated with pre-stroke and post-stroke dementia: a systematic review and meta-analysis. Lancet Neurol 2009; 8: 1006–18.
Penfield W. Neuroglia and microglia: the interstitial tissue of the central nervous system. In: Cowdry EV, editors. Special cytology: the form and functions of the cell in health and disease. New York: Paul B. Hoeber; 1928. p. 1033–1068.
Perry RH, Oakley AE. 'Newcastle brain map'. Neuropsychiatric disorders. London: Wolfe; 1993. p. 1–10.
Popescu BF, Bunyan RF, Guo Y, Parisi JE, Lennon VA, Lucchinetti CF. Evidence of aquaporin involvement in human central pontine myelinolysis. Acta Neuropathol Commun 2013; 1: 40.
Popescu BF, Parisi JE, Cabrera-Gomez JA, Newell K, Mandler RN, Pittock SJ, et al. Absence of cortical demyelination in neuromyelitis optica. Neurology 2010; 75: 2103–9.
Qin AP, Liu CF, Qin YY, Hong LZ, Xu M, Yang L, et al. Autophagy was activated in injured astrocytes and mildly decreased cell survival following glucose and oxygen deprivation and focal cerebral ischemia. Autophagy 2010; 6: 738–53.
Robinson CA, Adiele RC, Tham M, Lucchinetti CF, Popescu BF. Early and widespread injury of astrocytes in the absence of demyelination in acute haemorrhagic leukoencephalitis. Acta Neuropathol Commun 2014; 2: 52.
Sahlas DJ, Bilbao JM, Swartz RH, Black SE. Clasmatodendrosis correlating with periventricular hyperintensity in mixed dementia. Ann Neurol 2002; 52: 378–81.
Savva GM, Stephan BC. Epidemiological studies of the effect of stroke on incident dementia: a systematic review. Stroke 2010; 41: e41–6.
Sjobeck M, Haglund M, Englund E. Decreasing myelin density reflected increasing white matter pathology in Alzheimer's disease–a neuropathological study. Int J Geriatr Psychiatry 2005; 20: 919–26.
Smallwood A, Oulhaj A, Joachim C, Christie S, Sloan C, Smith AD, et al. Cerebral subcortical small vessel disease and its relation to cognition in elderly subjects: a pathological study in the Oxford Project to Investigate Memory and Ageing (OPTIMA) cohort. Neuropathol Appl Neurobiol 2012; 38: 337–43.
Taniguchi M, Yamashita T, Kumura E, Tamatani M, Kobayashi A, Yokawa T, et al. Induction of aquaporin-4 water channel mRNA after focal cerebral ischemia in rat. Brain Res Mol Brain Res 2000; 78: 131–7.
Tomimoto H, Akiguchi I, Suenaga T, Nishimura M, Wakita H, Nakamura S, et al. Alterations of the blood-brain barrier and glial cells in white-matter lesions in cerebrovascular and Alzheimer's disease patients. Stroke 1996; 27: 2069–74.
Tomimoto H, Akiguchi I, Wakita H, Suenaga T, Nakamura S, Kimura J. Regressive changes of astroglia in white matter lesions in cerebrovascular disease and Alzheimer's disease patients. Acta Neuropathol 1997; 94: 146–52.
Tradtrantip L, Zhang H, Saadoun S, Phuan PW, Lam C, Papadopoulos MC, et al. Anti-aquaporin-4 monoclonal antibody blocker therapy for neuromyelitis optica. Ann Neurol 2012; 71: 314–22.
Vataja R, Pohjasvaara T, Mantyla R, Ylikoski R, Leppavuori A, Leskela M, et al. MRI correlates of executive dysfunction in patients with ischaemic stroke. Eur J Neurol 2003; 10: 625–31.
Wardlaw JM, Doubal F, Armitage P, Chappell F, Carpenter T, Munoz Maniega S, et al. Lacunar stroke is associated with diffuse blood-brain barrier dysfunction. Ann Neurol 2009; 65: 194–202.
Yamamoto Y, Ihara M, Tham C, Low RW, Slade JY, Moss T, et al. Neuropathological correlates of temporal pole white matter hyperintensities in CADASIL. Stroke 2009; 40: 2004–11.
Yamashita T, Kamiya T, Deguchi K, Inaba T, Zhang H, Shang J, et al. Dissociation and protection of the neurovascular unit after thrombolysis and reperfusion in ischemic rat brain. J Cereb Blood Flow Metab 2009; 29: 715–25.